Class Specific Physical Properties of Liquid Crystals and Correlations with Molecular Structure and Static Electrooptical Performance in Twist Cells

M. Schadt and P. R. Gerber

F. Hoffmann-La Roche & Co., Ltd. Central Research Units, 4002 Basel, Switzerland

Z. Naturforsch. **37a**, 165–178 (1982); received February 3, 1982

For the 65th aniversary of Professor Walter Boguth

We made measurements of the temperature dependence of the static dielectric constants, the optical anisotropy and the three elastic constants of binary mixtures belonging to twelve structurally and physically markedly different liquid crystal classes. The class-specific material properties were quantitatively correlated with molecular structural elements. The changes of material properties occurring when different LC-classes are combined were investigated. Analytical approximations are presented which are shown to reproduce the static transmission characteristics of twisted nematic cells and their dependence on material constants and temperature with an accuracy comparable to exact numerical calculations. Strong smectic pretransitional effects are shown to influence not only k_{22} and k_{33} but also k_{11}, thus suggesting that not only twist and bend but also splay deformations may be prohibitive in smectics. We show that the elastic ratio k_{33}/k_{11} of different liquid crystal classes increases with increasing dielectric anisotropy thus leading to a decrease of the slope of transmission characteristics of twist cells. Furthermore, it is shown that k_{33}/k_{11} decreases for molecules comprising heterocyclic rings whereas hydrogenation of an aromatic ring causes k_{33}/k_{11} to increase.

1. Introduction

Some macroscopic liquid crystal (LC) material parameters such as the refractive indices or the dielectric constants may be related via appropriate models with molecular properties such as conjugated π-electron systems or permanent dipole moments. Based on structural considerations predictions for these material constants are possible especially for the optical properties. As a consequence molecular structures may be designed with specific optical and dielectric properties, for instance for applications in liquid crystal displays.

All electro-optical effects known in the field of nematic liquid crystals are based in one way or another on deformations of the nematic director under the influence of an applied voltage. The extent to which a liquid crystal layer can visibly be deformed depends not only on its dielectric and optical material constants but essentially also on its elastic properties giving rise to restoring forces. In general the elastic restoring forces can be described by three elastic constants, namely those for splay (k_{11}), twist (k_{22}) and bend (k_{33}) deformation.

Reprint requests to Dr. M. Schadt, F. Hoffmann-La Roche & Co., Limited Company, CH-4002 Basel.

Because of experimental difficulties and the rather extensive numerical data evaluation required, it was not until recently that reliable and complete measurements of all three elastic constants could be made. Perhaps due to the lack of data physical models do not exist that could be used to correlate the macroscopic elastic properties of liquid crystals with molecular structure. Therefore, molecular engineering of specific elastic properties based on experimental data or even semiquantitative models is not yet possible. Thus, the next step, namely the elaboration of correlations between LC-class specific material properties and their specific influence on the macroscopic electro-optical performance of field effects could hardly be made either. Furthermore, calculations describing the performance of electro-optical effects of liquid crystals quantitatively — which necessarily require complete sets of relevant material parameters — could be verified only for a few LC-materials. It was not until recently that efforts were made to investigate, besides negative dielectric liquid crystals [1, 2], complete sets of material parameters of positive dielectric substances also [3–7].

To our knowledge only one attempt has been made to determine and compare the relevant material properties of different positive dielectric

0340-4811 / 82 / 0200-0165 $ 01.30/0. — Please order a reprint rather than making your own copy.

liquid crystal classes [7] and to relate them with some aspects of the electro-optical performance of the twisted nematic effect. Investigations into the interactions that occur when different classes of substances are combined, the consequent changes of the material properties of such mixtures and their effects on the electro-optical performance of field-effects have not yet been reported. In the attempt to study such interactions, to make qualitative correlations with molecular structures and to relate the class specific material properties quantitatively with the static electro-optical performance of twisted nematic displays (TN-LCDs) [8], we have complemented and extended our previous measurements [7] to new LC-classes as well as to combinations of components belonging to twelve different classes which differ markedly, both with respect to molecular structure as well as with respect to their dielectric, optical and elastic properties. The influence of different structural elements and/or combinations of different structures on the measured temperature dependence of the dielectric, optical and all three elastic constants was investigated. To correlate the class specific material properties with a macroscopic electro-optical effect, measurements of the static transmission characteristic of the TN-LCDs were made. Analytical approximations describing the transmission characteristics of TN-LCDs as functions of LC-material constants were derived. They were shown to reproduce essential aspects of the experimentally determined characteristics with a high degree of accuracy comparable to that obtained from complex numerical calculations. Measurements of the class specific influence on the dynamics of TN-LCDs will be presented in a following article.

2. LC-Classes and Experimental Procedure

The liquid crystals chosen cover a wide range of dielectric and optical anisotropies ($-1 \lesssim \Delta\varepsilon \lesssim 25$; $0.07 \lesssim \Delta n \lesssim 0.25$); i.e. ranges into which most substances fall that can be made today. Table 1 shows their molecular structures. With one exception the rigid part of the molecules contains two rings which are either linked directly or via different linking bonds. Furthermore, molecules with

	Composition	Mol. Prop.	Structure	Ref.
E	(E5, E7)	(40, 60)	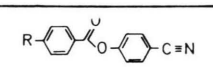	[9]
S	(S5, S7)	(40, 60)	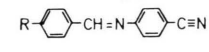	[10]
K	(K15, K21)	(40, 60)	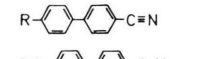	[11]
M	(M15, M21)	(40, 60)	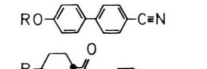	[11]
PE	(PCHE5, 7)	(40, 60)	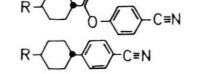	[12]
PC	(PCH5, 7)	(40, 60)	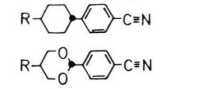	[13]
PD	(PD5, 7)	(40, 60)	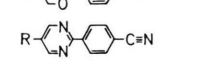	[14]
P	(P_35, P_37)	(40, 60)	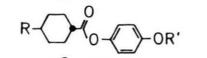	[15]
EC	($3EH_2O2$, $3EH_2O4$)	(40, 60)	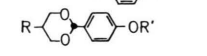	[12]
PDO	(5PDO2, 5PDO4)	(40, 60)		[14]
P_{82}	(P_37, $5EH_2O3$)	(80, 20)		
P_{64}	(P_37, $5EH_2O3$)	(60, 40)		
P_{28}	(P_37, $5EH_2O3$)	(20, 80)		
T_{28}	(TP_3H_37, $5EH_2O3$)	(20, 80)	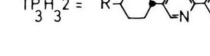	[16]
P_{pd}	(P_37, PD5)	(60, 40)		
P_{pdo}	(P_37, 5PDO3)	(60, 40)		
P_{pc}	(P_37, PCH5)	(60, 40)		
P_{mb}	(P_37, MBBA)	(60, 40)	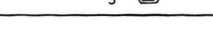	

Table 1. Nomenclature, composition and chemical structures of the pure class-specific binary mixtures (upper 10) and of binaries comprising components belonging to different LC-classes (bottom 8); R = pentyl or hexyl respectively.

polar and nonpolar end groups as well as with aromatic, hydrogenated or heterocyclic rings are used. The different structural elments are chosen such that the physical changes occuring in the material- and electro-optical properties can hopefully be related with them.

As some of the LC-components investigated exhibit rather narrow non-overlapping mesomorphic ranges or are even monotropic, binary mixtures were made to enlarge the mesomorphic ranges. Exept for binaries containing components which do not belong to the same LC-class, all positive dielectric mixtures contained a pentyl and a heptyl component in molar proportions (40%, 60%). Thus, effects on the material properties due to unequal proportions or unequal chain lengths which affect the dielectric [15] as well as the elastic [2] properties within homologous series could be omitted. The abbreviations and the corresponding compositions of the binary mixtures are depicted in Table 1 where R and R' designate alkyl chains. For example E5 stands for pentyl cyano ester. Their mesomorphic properties including melting (T_m), smectic A-nematic (T_{sn}) and nematic-isotropic (T_c) transition temperatures are depicted in Table 3 below.

The lower part of Table 1 shows 8 binary mixtures consisting of components which belong to different LC-classes and are combined in different molar proportions. Most of these mixtures contain a 2-paracyanophenyl-heptylpyrimidine as one component designated by a capital P in the respective mixture denomination. These two-class binaries are used to show the effects of one LC-class — namely pyrimidines — on the material parameters of other classes or vice versa.

The experimental details or references to the methods used to determine the static dielectric constants, the optical anisotropies, the static electro-optical transmission characteristics of TN-LCDs and the cell preparation were described earlier [3]. The three elastic constants were determined by optically detecting the magnetic-field-induced deformations of the nematic director of homogeneously aligned LC-layers. Numerical fitting procedures were used to evaluate the results. The twist elastic constants were measured by means of a recently described method [17]. A detailed description of the accurate ($\pm 3\%$) measuring techniques used to determine k_{11}, $k_{22}$and k_{33} were described recently [17].

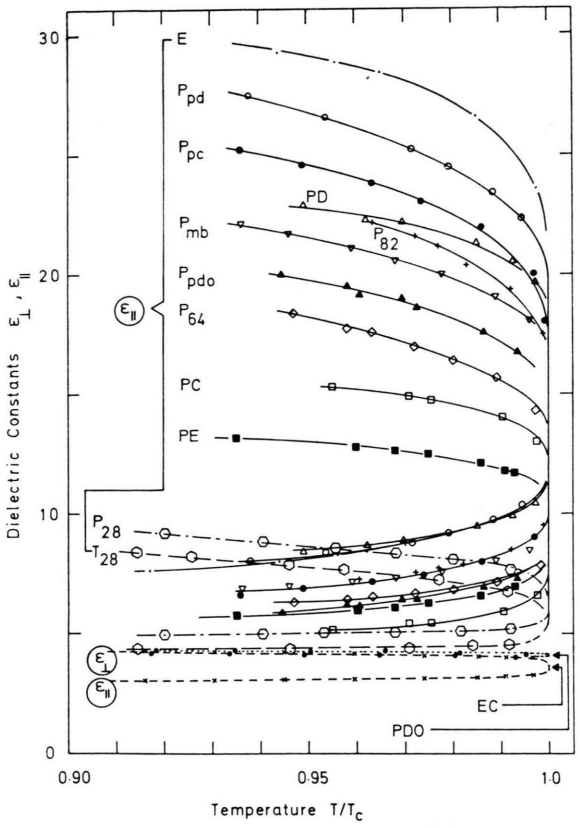

Fig. 1. Measurements of the temperature dependence of the static dielectric constants $\varepsilon_{\parallel}$ and $\varepsilon_{\perp}$.

3. Class-Specific Material Properties

3.1. Dielectric Constants

Figure 1 shows measurements of the temperature dependence of the static dielectric anisotropy $\Delta\varepsilon = (\varepsilon_{\parallel} - \varepsilon_{\perp})$ of those binary mixtures in Table 1 for which the respective data were not yet published in reference [7]. Except for mixture EC all others exhibit a positive dielectric anisotropy (Figure 1). Table 2 summarizes the dielectric data of all mixtures measured at constant temperature (T_c — 10 °C) corresponding to a reduced temperature $(T_c - 10\ °C)/T_c \cong 0.97 = \text{constant}$.

Among the 10 single-class mixtures in Table 1 P and E exhibit — with $\Delta\varepsilon \cong +20$ — the largest positive dielectric anisotropies, followed by a number of mixtures with $\Delta\varepsilon \cong +10$ and the barely positive anisotropic mixture PDO, whereas $\Delta\varepsilon$ of EC is slightly negative (Fig. 1, Table 2). From $\Delta\varepsilon(\text{PD}) \cong 13$ and $\Delta\varepsilon(\text{PDO}) \cong 0$ in Table 2 follows

Table 2. Measurements of the elastic, dielectric and optical material properties made at constant temperature ($T_c - 10\,°C$).

LC	k_{11} ($\times 10^{-12}$ N)	k_{22} ($\times 10^{-12}$ N)	k_{33} ($\times 10^{-12}$ N)	k_{33}/k_{11}	k_{22}/k_{11}	$\Delta\varepsilon$	$\varepsilon_\perp$	$\Delta\varepsilon/\varepsilon_\perp$	Δn	n_0
E	6.05	3.62	10.10	1.67	0.60	19.74	8.73	2.263	0.149	1.504
S	6.25	3.16	8.70	1.39	0.51	13.30	7.60	1.750	0.204	1.529
K	6.70	3.60	9.00	1.34	0.54	11.73	6.05	1.939	0.177	1.526
M	5.15	3.10	6.40	1.24	0.60	9.90	6.95	1.425	0.168	1.521
PE	5.50	3.16	8.50	1.55	0.57	6.40	6.20	1.032	0.086	1.469
PC	6.75	3.30	10.50	1.56	0.49	9.69	5.21	1.860	0.097	1.484
PD	4.90	3.14	7.00	1.43	0.64	13.30	8.90	1.495	0.089	1.480
P	7.00	3.86	8.10	1.16	0.55	19.72	8.71	2.263	0.183	1.516
EC	6.20	3.43	7.95	1.28	0.55	−.96	4.14	−.232	0.073	1.468
PDO	7.95	3.89	6.75	0.85	0.49	0.12	4.08	0.029	0.075	1.476
P_{pd}	5.90	3.38	6.70	1.14	0.57	16.70	8.70	1.919	0.133	1.501
P_{pdo}	8.50	4.44	6.45	0.76	0.52	12.60	6.20	2.032	0.130	1.497
P_{pc}	6.70	3.54	8.40	1.25	0.53	16.15	7.35	2.197	0.133	1.503
P_{mb}	7.40	4.00	6.80	0.92	0.54	13.30	7.30	1.822	0.167	1.529
P_{82}	6.65	3.66	6.15	0.92	0.55	14.30	7.50	1.907	0.133	1.505
P_{64}	6.70	3.12	6.05	0.90	0.47	10.50	6.60	1.591	0.119	1.495
P_{28}	6.60	2.92	5.20	0.79	0.44	3.30	5.00	0.660	0.077	1.478
T_{28}	5.90	3.16	5.00	0.85	0.54	2.95	4.35	0.678	0.071	1.469

that the large dielectric anisotropy of PDs is essentially due to their longitudinal permanent dipole moments of the cyano end groups.

At first it is astonishing to note the considerable difference between the values of $\varepsilon_\perp$ and $\Delta\varepsilon$ of the structurally similar esters E and PE in Table 2. From the dielectric theory of Maier and Meier [18] the differences have to be explained either by a smaller dipole moment of PE compared with E which in addition lies off the long molecular axis or by markedly different reaction field- and cavity factors. Considering the electron affinity of cyano- and ester groups and the ability of aromatic rings to release electrons, the first explanation appears quite plausible. Accordingly, mesomeric interactions in the aromatic esters E which cause the displacement of π-electrons from the left aromatic ring of E (Table 1) towards the electron-acceptor oxygen double bond in the ester linkage lead to cummulative dipole moments in E's; whereas in PE's — due to the single aromatic ring — induced electron shifts lead to oppositely polarized dipole moments, thus causing $\Delta\varepsilon$(PE) to decrease.

The above findings show that predictions of the dielectric properties of the liquid crystalline state based on structural considerations may in some cases be rather difficult. However, if the dielectric properties of an LC-class are experimentally verified, predictions with respect to the changes that occur upon blending different classes are possible. From the measurements in Fig. 1 and Table 2 follows that the dielectric anisotropy $\Delta\varepsilon_{a,b}$ of a mixture containing components a and b that belong to different LC-classes is given in a first approximation by

$$\Delta\varepsilon_{a,b} \cong m_a \Delta\varepsilon_a + m_b \Delta\varepsilon_b;$$
$$m_a + m_b = 1. \qquad (1)$$

m_a and m_b are the respective molar proportions and $\Delta\varepsilon_a$ and $\Delta\varepsilon_b$ the dielectric anisotropies of the single-class mixtures a and b. The measurments in Table 2 show that a relation analogous to (1) holds for $\varepsilon_\perp$. As an example the dependence of $\Delta\varepsilon$ on different blending ratios made among mixtures P and EC is shown in Figure 2. The normalized measuring points (circles) follow from the respective values of $\Delta\varepsilon$ of mixtures P, P_{82}, P_{64}, P_{28} and EC in Table 2. The deviations of the measured $\Delta\varepsilon$-values for large concentrations of P_37 in mixtures (P_37, $5EH_2O3$) from the linear solid line in Fig. 2 are probably due to the lower $\Delta\varepsilon$-values of P_37 compared with those of P_35 [15] used in the normalizing mixture P = (P_35, P_37).

3.2. Refractive Indices

Figure 3 shows measurements of the temperature dependence of the ordinary and extraordinary refractive indices n_0 and n_e of those binary mixtures not investigated in reference [7]. Table 2 contains data of the birefringence $\Delta n = (n_e - n_0)$ and of n_0

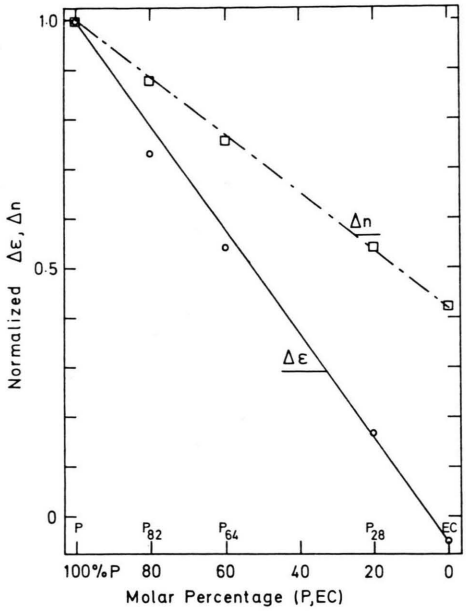

Fig. 2. Plot of the normalized dielectric anisotropy $\Delta\varepsilon = \Delta\varepsilon(\mathrm{P, EC})/\Delta\varepsilon(\mathrm{P})$ for different molar proportions following from the respective measurements of $\Delta\varepsilon$ in Table 2 for mixtures P, P_{82}, P_{64}, P_{28} and EC (solid line). The dashed graph shows the analogous dependence for the respective optical anisotropies Δn.

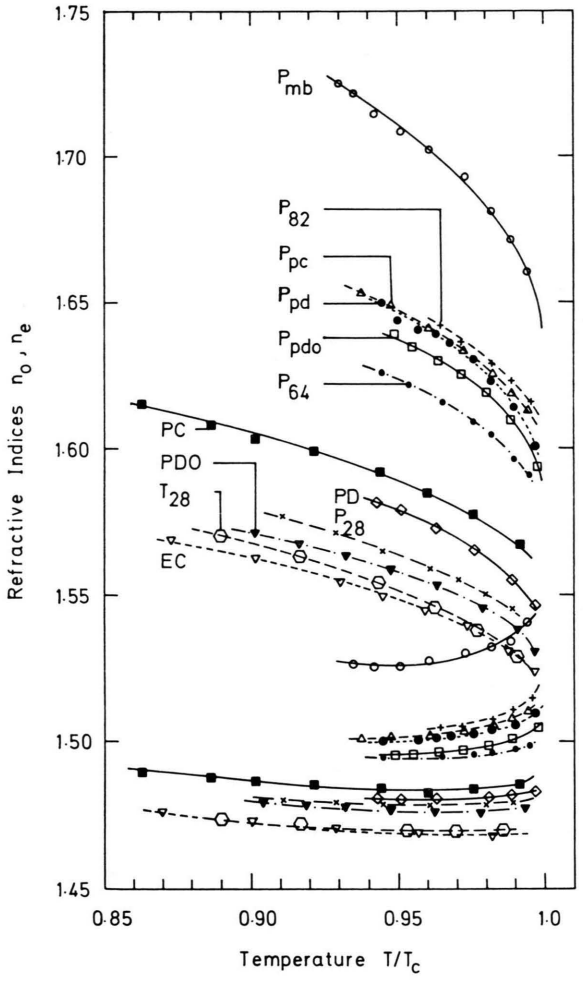

Fig. 3. Measurements of the temperature dependence of the ordinary and extraordinary indices of refraction n_o and n_e.

of all mixtures measured at $(T_c - 10\ °C) = \text{constant}$. The largest optical anisotropies in Table 2 correspond to compounds with elongated and highly conjugated π-electron systems such as Schiff'bases S. Shorter or less conjugated molecules such as biphenyls K or aromatic esters E exhibit lower values of Δn; whereas the lowest optical anisotropies correspond as expected to the partially hydrogenated compounds PC, PE, EC, PD and PDO (Table 2). Thus, the optical anisotropies of all LC-classes investigated can at least qualitatively be predicted based on individual molecular properties.

In analogy to (1) the resulting birefringence of mixtures comprising components belonging to different LC-classes can rather accurrately be determined for a given mixing ratio. This is illustrated by the dashed graph in Fig. 2 where the measurements were taken from Table 2.

3.3. Elastic Constants k_{11}, k_{22} and k_{33}

In the following, measurements of the temperature dependence of the splay (k_{11}), twist (k_{22}) and bend (k_{33}) elastic constants are reported. Figure 4 shows measurements of $k_{11}(T)$, whereas those for $k_{22}(T)$ and $k_{33}(T)$ are depicted in Figs. 5 and 6 respectively. Except for T_{28} (Table 1) all binaries in Figs. 4—6 belong to the single-class type, whereas the measurements depicted in Figs. 7 and 8 were made — except for PDO and EC — with binaries containing components belonging to different classes; i.e. with two-class mixtures. For reference purposes the data for mixture P are included in Figs. 7 and 8. For a few of the mixtures measurements were reported earlier using electric-field realignment and a capacitive detection method to determine k_{11} and k_{33} [7]. Since then numerical evaluation methods and improved measuring tech-

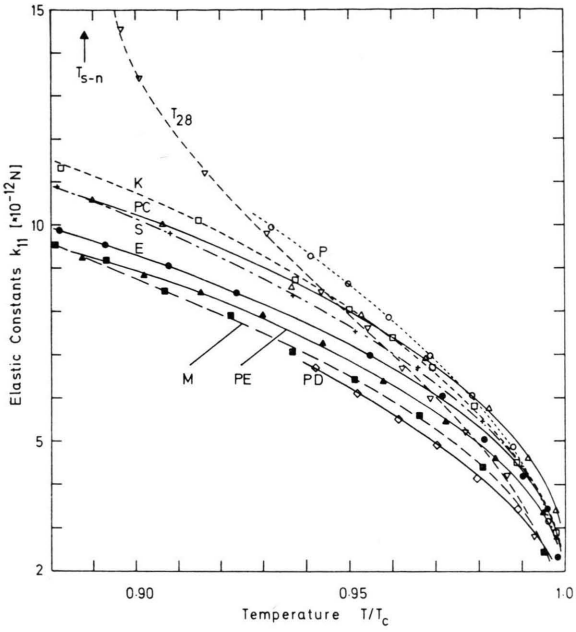

Fig. 4. Measurements of the splay elastic constants k_{11} versus reduced temperature T/T_c.

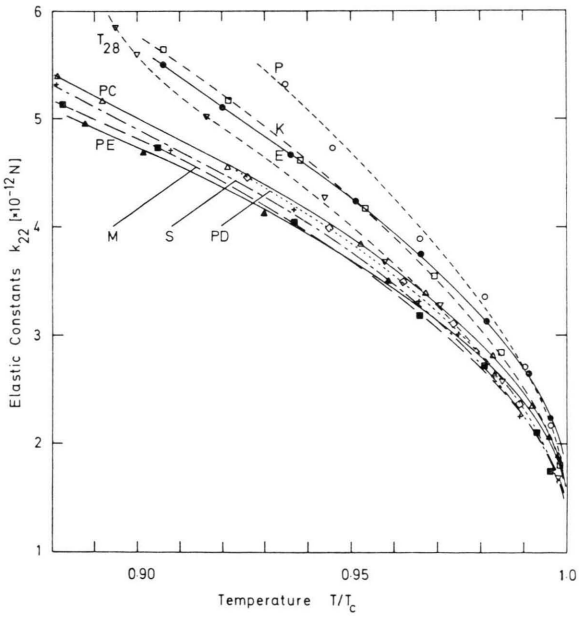

Fig. 5. Measurements of the twist elastic constants k_{22} versus reduced temperature T/T_c.

niques — especially to determine k_{33} — have been developed [17]. Thus, the more accurate ($\pm 3\%$) recent results for these few mixtures are also included in Figs. 4 and6.

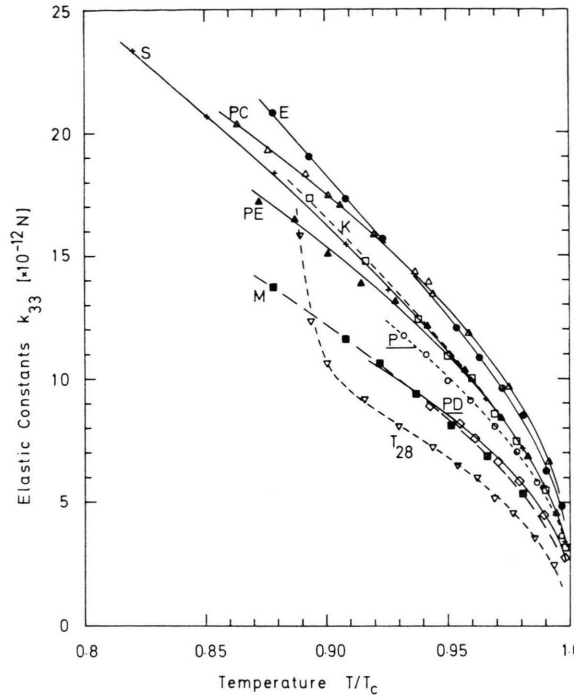

Fig. 6. Measurements of the bend elastic constants k_{33} versus reduced temperature T/T_c.

When looking at the temperature dependence $k_{ii}(T/T_c)$ depicted in Figs. 4—6 one gets the impression that the variations among $k_{11}(T/T_c)$ and $k_{22}(T/T_c)$ are small for the single-class mixtures. Even the graphs of k_{33} which exhibit the largest variations appear to fit onto each other when scaled appropriately. In contrast to this finding Figs. 7 and 8 show that the two-class mixtures exhibit a much larger variety of the shape of $k_{ii}(T/T_c)$ despite they all consist of 60% P_37. This different behaviour offers potentially the possibility to design mixtures exhibiting a relatively weak temperature dependence of the elastic constants which is desirable for many electro-optical applications.

The measurements depicted in Fig. 9 show the influence of temperature on the elastic ratios k_{33}/k_{11} and k_{22}/k_{11} for some binaries. Evidently the temperature dependence of k_{33}/k_{11} is low for all substances investigated. A similarly low temperature dependence was found for k_{22}/k_{11} for most compounds except for those with smectic phases and to some extent also for the phenyl dioxanes PD and PDO (Figure 9). Besides, the measurements in Fig. 9 show large LC-material specific variations of

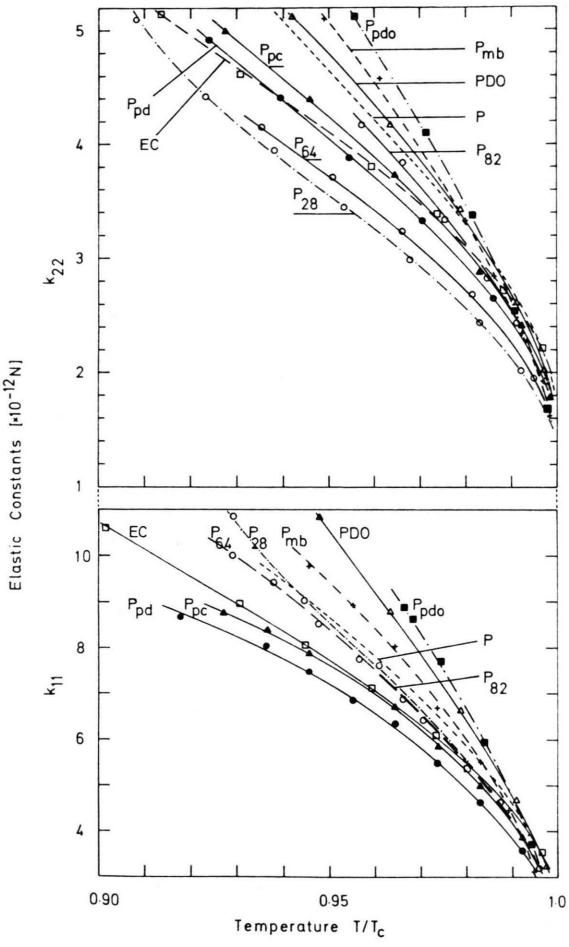

Fig. 7. Measurements of the splay and twist elastic constants versus reduced temperature made mainly with non-class-specific mixtures.

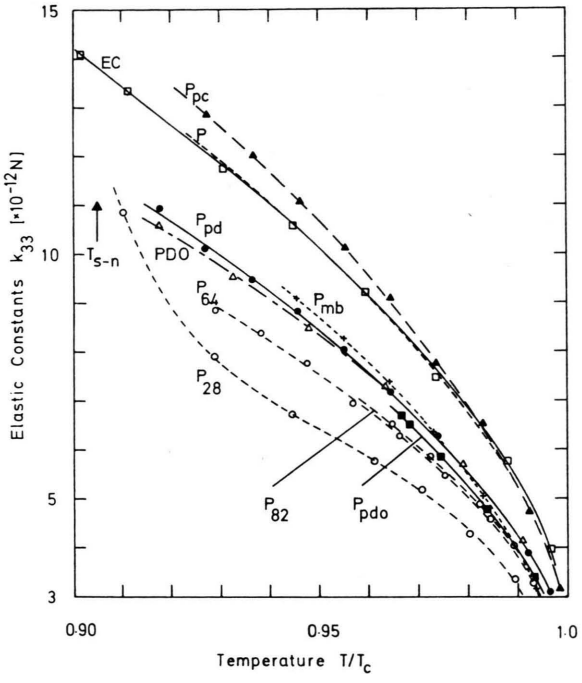

Fig. 8. Measurements of the bend elastic constants versus reduced temperature made with the same mixtures as in Figure 7.

k_{33}/k_{11} covering a range from ~ 0.7 to ~ 2.0. Therefore, if one assumes that the variations of k_{33}/k_{11} reported for two homologous series [2, 4] are typical for nematics, it seems possible to achieve ratios of k_{33}/k_{11} ranging from ~ 0.7 to ~ 3.0 by properly combining different LC-classes and homologues.

3.4. Smectic Pretransitional Effects

Because of the incompatibility of elastic twist- and bend deformations with smectic structures [19] the elastic constants k_{22} and k_{33} are expected to increase in the nematic phase of liquid crystals when approaching a smectic-nematic transition temperature T_{sn}. Our measurements made with mixtures P_{28} and T_{28} which both exhibit smectic A-nematic transitions (Table 3) indeed show pronounced increases of k_{22} and k_{33} in the nematic phase for temperatures approaching T_{sn} (Figures 5—8). Besides the measurements of $k_{11}(T)$ made with mixtures P_{28} and T_{28} in Figs. 4 and 7 show as a surprise that not only k_{22} and k_{33} but also k_{11} exhibits a pretransitional behaviour. Because splay deformations were so far thought to be compatible with the layer structure of smectic A phases it was generally expected that k_{11} should not show such a pretransitional behaviour. The astonishingly strong increase of $k_{11}(T \rightarrow T_{sn})$ which we found in P_{28} and T_{28} can best be seen in the representation of k_{33}/k_{11} and k_{22}/k_{11} versus temperature in Figure 9. k_{22}/k_{11} steadily decreases for $T \rightarrow T_{sn}$ without any evidence of a pretransitional upward bending which one would expect if only $k_{22}(T \rightarrow T_{sn})$ would diverge; whereas k_{33}/k_{11} shows a rather minor increase very close to T_{sn}. Thus, if the pretransitional behaviour of k_{22} and k_{33} should differ from that of k_{11} the difference would have to occur in a very narrow temperature intervall near T_{sn}. Therefore, our measurements suggest that pretransitional smectic tendencies affect all three elastic deformations similarly.

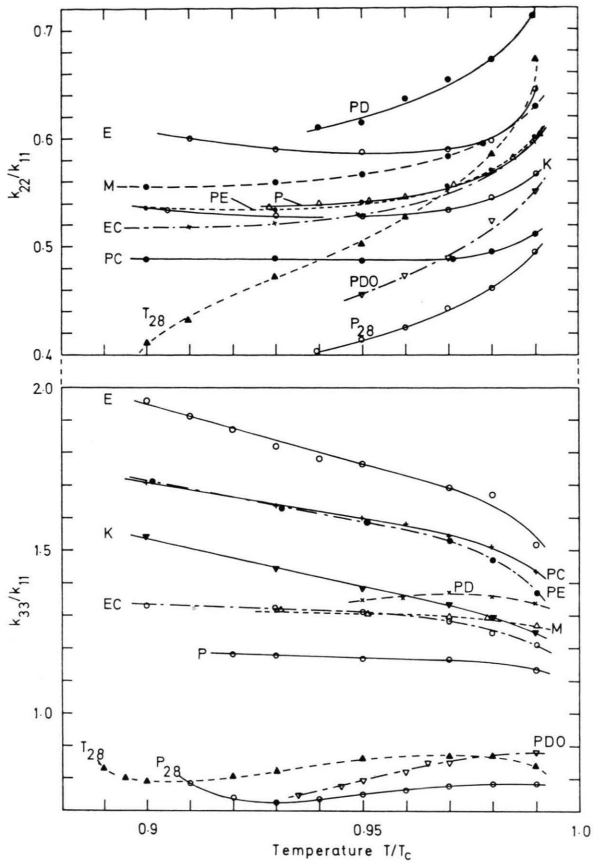

Fig. 9. Temperature dependence of k_{33}/k_{11} and k_{22}/k_{11} following from the measurements depicted in Figures 4—8.

3.5. Structural and Blending Effects on k_{ii}

Table 2 summarizes all elastic data measured at constant temperature ($T_c - 10$ °C); i.e. far from any smectic-nematic transition temperature of the mixtures used (Table 1, Table 3). The elastic ratios k_{22}/k_{11} show only minor variations of $\pm 10\%$ among different liquid crystal materials (Table 2). Therefore, we shall concentrate our discussion of structural effects on the ratio k_{33}/k_{11} which was found to vary appreciably and in a significant manner (Table 2).

The mixtures were chosen such that effects due to different alkyl chain lengths can be expected to be very similar in all of them. Variations of material parameters among different binaries can therefore be attributed to other molecular structural elements. We deduct from the measurements of k_{33}/k_{11} in Table 2 the following interpretation of the dependence of k_{33}/k_{11} on molecular structure and polarity: (i) k_{33}/k_{11} is closely correlated with the polarity of the molecules; i.e. with $\Delta\varepsilon$, (ii) hydrogenation of one ring causes k_{33}/k_{11} of the hydrogenated compound to increase by $\delta_1 \cong 0.41$ compared with its aromatic counterpart and (iii) the introduction of two heteroatoms into a hydrogenated ring (oxygens in the cyclohexyl rings of phenyldioxanes PD and PDO) or in an aromatic ring (nitrogens in pyrimidines P) causes k_{33}/k_{11} of the heterocyclic compound to decrease by $\delta_2 \cong -0.45$ compared with its non-heterocyclic aromatic counterpart. These findings are visuallized in Fig. 10 where measured k_{33}/k_{11}-data from Table 2 — reduced if structurally required by the postulated corrections δ_1 and δ_2 — are plotted against the respective dielectric anisotropies of the binaries. The reduced elastic ratios are denominated by $\varkappa$ to distinguish them from the actually measured k_{33}/k_{11}-data in Table 2. The upper straight line in Fig. 10 shows the excellent correlation obtained for the single-class mixtures.

Our measurements made with the two-class mixtures in Table 2 show that mixing components of different liquid crystal classes leads to a depression of k_{33}/k_{11} compared with the values which one would expect from a linear interpolation of k_{33}/k_{11} of the respective single-class data (compare for instance k_{33}/k_{11} of the two-class mixture P_{82} with k_{33}/k_{11} of the respective single-class mixtures P and EC in Table 2 which are both larger than k_{33}/k_{11} of P_{82}). The corrected and weighted values of k_{33}/k_{11} of the two-class mixtures lead to the $\varkappa$-values depicted in Figure 10. $\varkappa$ was determined by correcting each of the components X and Y with the corresponding structural factors δ (if required) and by weighting the amounts of the components used in the mixture with the respective molar proportions m according to the following equation:

$$\varkappa_{x,y} = k_{33}/k_{11} - m_x \delta_x - m_y \delta_y; \quad m_x + m_y = 1. \tag{2}$$

Equation (2) not only holds for two-class mixtures but is applicable to single-class mixtures also if one inserts $m_x = 1$ and $m_y = 0$.

Figure 10 shows that the $\varkappa$-values of the two-class mixtures — like those of the single-class mixtures — fit well on a straight line, thus indicating that the assumed correlations between k_{33}/k_{11}, structural- and dielectric properties apply also in the two-class binaries investigated. The increased

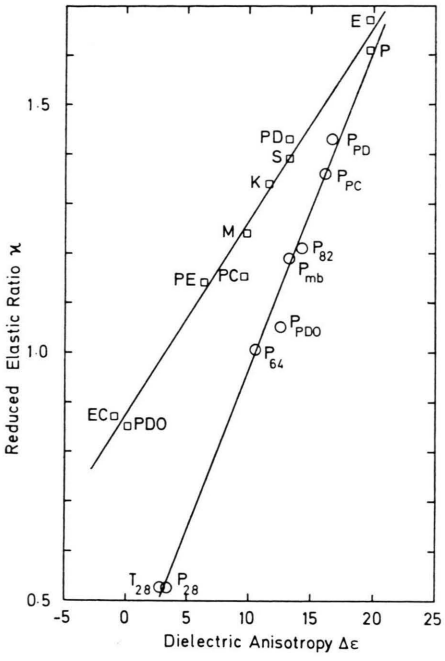

Fig. 10. Reduced parameter $\varkappa$ following from weighted and corrected measurements of k_{33}/k_{11} (c.f. (2)) of single- and two-class mixtures versus $\Delta\varepsilon$.

slope of the lower graph in Fig. 10 may be due to the somewhat longer alkyl chains used in P_{28}, P_{64}, P_{82} and P_{PDO} compared with the corresponding single-class mixtures. Surprisingly mixture T_{28} — which is the only one comprising a three ring component — fits the line for the shorter two-ring compounds very well too (Figure 10). This may be an indication that the postulate, according to which increased molecular length/width ratios lead to an increase of k_{33}/k_{11} [5], may not hold generally.

Despite the good correlation found between the corrected and weighted k_{33}/k_{11}-values in the above two-class mixtures, care should be taken when applying our results to other two-class mixtures comprising components with structural elements not investigated here. Since such structural elements may affect the ratio k_{33}/k_{11} in an analogous manner as found for heterocyclic or hydrogenated rings, additional structure-specific corrections δ may be required.

4. Analytical Approximations for Twist-Cell Transmission

The static electro-optical characteristics of a TN-LCD can be defined by a driving voltage V_{50} at which the transmission has reached 50% and by a parameter p characterizing its (linear) slope. p is defined as

$$p = (V_{50} - V_{10})/V_{10}, \tag{3}$$

where V_{10} is the driving voltage for 10% transmission. In the following we assume vertical incidence of light onto the display at wavelength λ and zero bias tilt angles of the LC-molecules at the electrode boundaries.

It was shown by Berreman [20] that elaborate numerical calculations are required to determine the field-induced deformation of the director pattern and the electro-optical transmission characteristics of twisted nematic cells. Due to the complex non-analytical calculations the influence of specific LC-material parameters such as dielectric, elastic and optical constants on the transmission characteristics of TN-LCDs is rather difficult to elaborate. Based on numerical calculations [21] we have therefore made an attempt to derive analytical approximations reproducing the main features of the dependence of the static transmission characteristics of TN-LCDs on LC-material and display parameters. In these calculations for which a computer programme from Berreman was used, the dependence of the parameter p in (3) on d/λ was investigated for systematically varying elastic and dielectric constants; d = display spacing. The graphical representation of the results suggested that a parabolic approximation can be used to describe the function $p(\ln[d/\lambda])$. By means of least mean square fitting we obtain the following approximation p^+ for the parameter p

$$p^+ = 0.1330 + 0.0266\left(\frac{k_{33}}{k_{11}} - 1\right) + 0.443\left(\ln\frac{\Delta n\, d}{2\lambda}\right)^2. \tag{4}$$

It will be shown in Sect. 5 that the dependencies of p^+ on the dielectric constants as well as on k_{22}/k_{11} which were disregarded when deriving equation (4) can indeed be neglected. Equation (4) suggests that the slope of the transmission characteristics of TN-LCDs depends essentially only on the elastic ratio k_{33}/k_{11} and on the optical path difference $\Delta n d/\lambda$. It was shown before [21] that the lowest p-values, i.e. the steepest slopes are obtained if the display spacing and/or the optical anisotropy

of the LC-material are chosen such that

$$\Delta n\, d/2\,\lambda = 1 \tag{5}$$

is fulfilled. This corresponds to the minimum of the parabola (4).

In analogy to the least mean square fitting procedure used to derive the above approximation for p we also derived an analytical approximation V_{50}^{+} for the driving voltage V_{50} using the results of the numerical calculations of V_{50}/V_c versus $\ln(d/\lambda)$ in [21]:

$$V_{50}^{+} = V_c \times \left[2.044 - \frac{1.044}{1 + k_{33}/k_{11}}\right] \times \left\{1 + 0.123\left[\left(\frac{\Delta\varepsilon}{\varepsilon_\perp}\right)^{0.6} - 1\right]\right\} \times \left(1 + 0.132 \ln \frac{\Delta n\, d}{2\,\lambda}\right). \tag{6}$$

V_c is the threshold voltage for the mechanical deformation of the helical structure in a TN-LCD. V_c can accurately be determined for instance from capacitance measurements [3]. In a TN-LCD with twist angle φ comprising a nematic LC-material doped with an optically active additive, V_c is given by

$$V_c = \pi\left[\frac{1}{\varepsilon_0 \Delta\varepsilon}\left\{k_{11} + (k_{33} - 2\,k_{22})\left(\frac{\varphi}{\pi}\right)^2\right\} + 2\,k_{22}\left(\frac{\varphi}{\pi}\right)\frac{2\,d}{\varrho}\right]^{1/2}. \tag{7}$$

In (7) ϱ is the natural pitch of the doped nematic. From (6) and (7) one obtains for a 90° twisted TN-LCD comprising a purely nematic LC-material, i.e. $\varrho = \infty$.

$$V_{50}^{+} = \pi \sqrt{\frac{k_{11}}{\varepsilon_0 \Delta\varepsilon}}\left[1 + \frac{k_{33}/k_{11} - 2\,k_{22}/k_{11}}{4}\right]^{1/2} \times \left[2.044 - \frac{1.044}{1 + k_{33}/k_{11}}\right] \times \left\{1 + 0.123\left[\left(\frac{\Delta\varepsilon}{\varepsilon_\perp}\right)^{0.6} - 1\right]\right\} \times \left(1 + 0.132 \ln \frac{\Delta n\, d}{2\,\lambda}\right). \tag{8}$$

The analytical approximation (8) suggests that unlike the slope of the transmission, V_{50} depends not only on k_{33}/k_{11} and on $\Delta n \cdot d$ but also on k_{22}/k_{11} as well as strongly on k_{11} and on the dielectric properties of the LC-material.

We will show in the next chapter that the above analytical approximation for p and V_{50} hold for all LC-classes investigated.

5. Material Constants and Electro-Optical Performance

5.1. Comparison Between Calculated and Measured TN-LCD Transmission

In the following measurements of the transmission characteristics of TN-LCDs are compared with those calculated by means of the analytical approximations of the preceding paragraph as well as with exact numerical calculations. The material parameters of Chapt. 3 obtained from measurements independent from those of the transmission characteristics of TN-LCDs are used in the calculations. TN-LCDs with 90° twist, zero bias tilt and spacings $d = 10$ μm were used ($\lambda = 550$ nm).

Figure 11 shows measured transmission characteristics of TN-LCDs comprising four different binary mixtures which cover a wide range of optical, dielectric and elastic properties (Table 2). The dashed graphs in Fig. 11 are those of the numerically calculated transmission characteristics using the material constants depicted in Table 2. Figure 11 shows that the agreement between calculated and measured transmission is better than 10% for all voltages and LC-materials; or vice versa: the driving voltage required for a given transmission

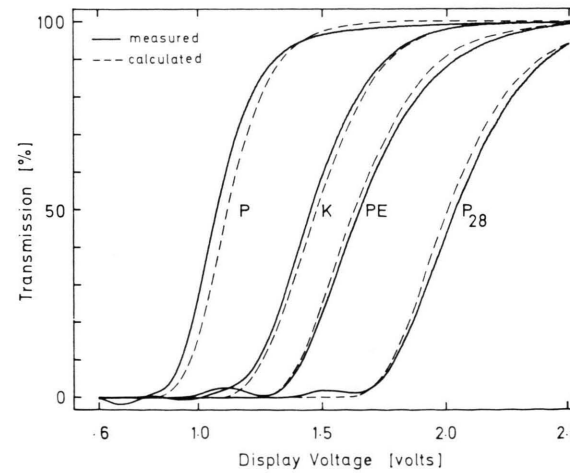

Fig. 11. Measured and numerically calculated transmission characteristics of TN-LCDs comprising the binary mixtures P, K, PE and P_{28} respectively. The recordings were made at $(T_c - 10\,°C) = \text{constant}$.

Table 3. T_m = melting temperature, T_{sn} = smectic A-nematic transition temperature and T_c = nematic-isotropic transition temperature. The data for the display driving voltages V_{10} and V_{50} and for the parameter p follow from measurements of the transmission characteristics of TN-LCDs performed at ($T_c - 10\,°C$) = constant. V_c = threshold voltage of the mechanical deformation of the helix calculated from (7) and the material constants in Table 2. V_{10}^*, V_{50}^* and p^* follow from numerical calculations; whereas V_{50}^+ and p^+ follow from the analytical approximations (4) and (8).

LC	T_m [°C]	T_{sn} [°C]	T_c [°C]	V_c [volts]	V_{10} [volts]	V_{50} [volts]	V_{10}^* [volts]	V_{50}^* [volts]	V_{50}^+ [volts]	p	p^*	p^+
E	25	—	56.2	0.618	1.004	1.154	1.007	1.159	1.145	0.149	0.151	0.155
S	< 0	—	70.7	0.757	1.146	1.346	1.159	1.373	1.381	0.175	0.184	0.160
K	< 0	—	39.4	0.824	1.250	1.444	1.281	1.490	1.484	0.155	0.162	0.152
M	~27	—	71.6	0.765	1.138	1.321	1.141	1.326	1.312	0.161	0.163	0.147
PE	~31	—	80.2	1.026	1.446	1.654	1.419	1.633	1.626	0.144	0.150	0.150
PC	3	—	55.6	0.943	1.384	1.580	1.405	1.603	1.600	0.142	0.141	0.148
PD	28	—	49.8	0.653	0.959	1.096	0.931	1.069	1.058	0.143	0.149	0.146
P	29	—	51.0	0.633	0.900	1.046	0.987	1.146	1.136	0.162	0.160	0.149
EC	<10	—	74.1	—	—	—	—	—	—	—	—	—
PDO	21	—	51.9	—	—	—	—	—	—	—	—	—
P_{pd}	28	—	49.8	0.627	0.982	1.119	0.940	1.072	1.058	0.139	0.141	0.138
P_{pdo}	20	34	48.8	0.836	1.209	1.359	1.194	1.344	1.320	0.124	0.126	0.128
P_{pc}	25	—	50.3	0.697	1.042	1.192	1.078	1.227	1.213	0.144	0.138	0.141
P_{mb}	~27	—	47.0	0.771	1.059	1.213	1.126	1.296	1.286	0.145	0.151	0.139
P_{82}	~38	—	50.0	0.704	1.030	1.163	1.026	1.167	1.147	0.129	0.137	0.133
P_{64}	~26	—	51.0	0.840	1.175	1.325	1.184	1.335	1.320	0.128	0.127	0.131
P_{28}	~22	29	61.0	1.475	1.846	2.058	1.792	2.009	1.996	0.115	0.121	0.133
T_{28}	~34	54	95.7	1.451	1.792	2.042	1.682	1.927	1.970	0.140	0.146	0.137

agrees within 4% between measurement and calculation. Thus, considering the experimental accuracy (3%) with which the transmission characteristics and the elastic constants could be determined, the overall agreement between calculation and experiment following from Fig. 11 is very good.

For all binary mixtures depicted in Table 1 we have measured the display driving voltages V_{10} and V_{50} at ($T_c - 10\,°C$) = constant as well as the parameter p defined by (3). The results are depicted in Table 3. To check the agreement between measured and calculated transmission characteristics of TN-LCDs for all LC-materials investigated, V_{10}, V_{50} and p were numerically calculated. The respective values in Table 3 are denominated V_{10}^*, V_{50}^* and p^*. Also depicted in Table 3 are V_{50}^+ and p^+ following from the analytical approximations (4) and (8). The material constants of Table 2 were used for the numerical and the analytical calculations. Comparing the measured values of the parameter p in Table 3 with the corresponding calculated parameters p^* and p^+ respectively shows that the maximum deviation between p and p^* is 8%, whereas p^+ agrees within 11% with p. The analytical approximation (4) thus leads to results whose accuracy is comparable to that of the much more complex numerical calculations.

A comparison between the numerically calculated driving voltages V_{10}^* and V_{50}^* in Table 3 with those determined experimentally shows that the agreement is better than 5% for all LC-classes investigated. Table 3 also shows that the same agreement was obtained between V_{50} and V_{50}^+. These findings show that the electro-optical transmission characteristics of TN-LCDs at vertical light incidence can indeed be accurately determined for virtually any LC-material from the above analytical approximations and from measurements of the dielectric, optical and elastic material constants; i.e. from k_{33}/k_{11}, Δn, $\Delta\varepsilon/\varepsilon_\perp$ and V_c when using (4) and (6).

5.2. Influence of Temperature on the Transmission of TN-LCDs

In the following the analytical approximations of Chapt. 4 will be used together with the measured temperature dependence of the material constants of chapter 3 to determine the parameters influencing the temperature dependence of the transmission characteristics of TN-LCDs. The strongly different binary mixtures K and E were chosen to show the effects to temperature on the characteristics.

Table 4 contains the material constants of mixtures K and E measured at different reduced tem-

Table 4. Elastic, dielectric and optical material constants of mixtures K and E measured at different reduced temperatures T/T_c. V_c and V_{50}^+ were calculated by inserting the respective material constants into (7) and (8).

T/T_c	k_{11} [$\times 10^{-12}$ N]	k_{22} [$\times 10^{-12}$ N]	k_{33} [$\times 10^{-12}$ N]	k_{33}/k_{11}	$\Delta\varepsilon$	$\Delta\varepsilon/\varepsilon_\perp$	Δn	V_c [volts]	V_{50}^+ [volts]
0.99 (K)	4.40	2.50	5.50	1.25	9.40	1.382	0.149	0.733	1.236
(E)	4.35	2.70	6.50	1.49	16.90	1.656	0.125	0.552	0.953
0.98	5.85	3.06	7.30	1.25	10.55	1.661	0.164	0.806	1.399
	5.30	3.18	8.40	1.58	18.40	2.022	0.138	0.593	1.067
0.97	6.75	3.50	8.70	1.29	11.30	1.852	0.174	0.841	1.495
	6.05	3.60	10.00	1.65	19.50	2.241	0.149	0.621	1.148
0.95	8.00	4.28	11.20	1.40	12.40	2.175	0.191	0.882	1.634
	7.25	4.26	12.50	1.72	20.95	2.570	0.162	0.662	1.265
0.94	8.70	4.60	12.30	1.41	12.85	2.315	0.198	0.907	1.701
	7.50	4.56	13.70	1.83	21.50	2.704	0.168	0.669	1.303
0.92	9.80	5.21	14.50	1.48	13.58	2.562	0.209	0.942	1.814
	8.60	5.10	16.10	1.87	22.40	2.909	0.176	0.708	1.403
0.90	10.75	5.76	16.50	1.53	14.05	2.702	0.218	0.976	1.910
	9.30	5.64	18.30	1.97	23.05	3.073	0.184	0.731	1.478

peratures T/T_c. By inserting these values into (7) and (8) respectively one obtains the values for V_c and V_{50}^+ depicted in the last two columns of Table 4. The calculated values of V_c are also depicted in the bottom part of Fig. 12 together with the measured temperature dependence of the threshold voltage determined in TN-LCDs by a capacitive detection method [3] (solid lines). Comparing the calculated temperature dependence of V_c with the one determined directly in TN-LCDs shows excellent agreement (bottom part of Figure 12). A comparably good agreement was found between the temperature dependence of $V_{50}(T/T_c)$ obtained from transmission measurements in TN-LCDs (solid graphs in the upper part of Fig. 12) and the calculated dependence $V_{50}^+(T/T_c)$ following from Table 4 (dashed graphs in Figure 12). These results show that the measured material constants and (7) and (8) reproduce the temperature dependence of the transmission characteristics of TN-LCDs well.

To separate the influence of the temperature dependence of the elastic, the dielectric and the optical material parameters on the transmission characteristics of TN-LCDs we have calculated $[V_{50}^+(T/T_c)]_x$ of mixture E from equation (8) for $(T/T_c = 0.99) = \text{constant}$, where x corresponds to the respective parameters $k_{11}(T/T_c = 0.99)$, $\Delta\varepsilon(T/T_c = 0.99)$ or $\Delta n(T/T_c = 0.99)$ in Table 4. Thus, one obtains the three dashed-dotted graphs in the upper part of Fig. 12 for the temperature dependence $V_{50}^+(T/T_c)_x = \text{constant}$. The deviation of these graphs from the actual temperature dependence of V_{50} shows the extent to which k_{11}, $\Delta\varepsilon$ and Δn influence the temperature dependence of the transmission. From Fig. 12 follows that the temperature dependence of $k_{11}(T)$ influences $V_{50}(T)$ most, followed by $\Delta\varepsilon(T)$, whereas the influence of $\Delta n(T)$ is comparably small.

6. Conclusions

We have measured the temperature dependence of the class-specific material properties, namely the three elastic constants, the static dielectric properties and the optical anisotropies of binary mixtures belonging to twelve structurally and physically markedly different liquid crystal classes. An attempt was made qualitatively to relate material properties with molecular structure. Besides, we have investigated the changes of material properties occurring when different classes of liquid crystals are combined. The class-specific material properties and their temperature dependence were quantitatively correlated with measurements of the static electro-optical transmission characteristics of twisted nematic cells using numerical calculations. The analytical approximations derived to describe the transmission characteristics of twist cells were shown to reproduce the experimentally determined characteristics with a high degree of

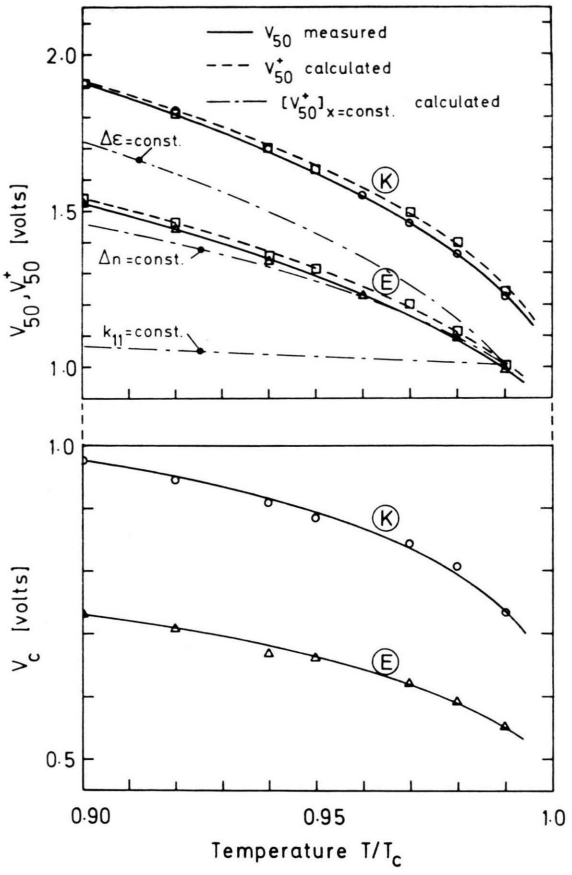

Fig. 12. Measured (solid lines) and calculated threshold voltages $V_c(T/T_c)$ of TN-LCDs using mixtures E and K respectively (bottom part of Figure 11). The upper part of the Figure shows the temperature dependence $V_{50}(T/T_c)$ (solid lines) obtained from transmission measurements of TN-LCDs for mixtures E and K. The dashed graphs (---) show the respective calculated dependencies $V^*_{50}(T/T_c)$ following from (8) and the measured temperature dependence of the material constants depicted in Table 4. The dashed-dotted graphs show the calculated temperature dependence of $[V^*_{50}]_{x=\text{constant}}$, where x corresponds to either of the parameters k_{11}, Δn or $\Delta\varepsilon$ measured at $T/T_c = 0.99 = \text{constant}$.

accuracy for all liquid crystals studied. They also show the degree to which the different material constants and their dependence on temperature influence the transmission characteristics.

From elastic measurements made in the nematic range of liquid crystals exhibiting a smectic A as well as a nematic phase we found strong smectic pretransitional effects to occur already at temperatures far above the smectic-nematic transition temperature. The pretransitional effects were found not only to affect twist and bend deformations strongly but also splay deformations. This finding is surprising considering that splay deformations have so far — in contrast to twist and bend — been supposed to be compatible with the smectic state.

We found large variations of k_{33}/k_{11} varying by a factor of 3 among different LC-classes at a given reduced temperature, whereas the measured variations of k_{22}/k_{11} were small. Our experiments show that hydrogenation of an aromatic ring in the core of two-ring LC-molecules causes the elastic ratio k_{33}/k_{11} to increase by the amount $\delta_1 = +0.41$, whereas substitution of an aromatic- or hydrogenated ring by a 1-3-substituted heterocyclic ring leads to a decrease of k_{33}/k_{11} by $\delta_2 = -0.45$. By taking the effects of different ring structures into account we have found an excellent correlation between the polarity of LC-molecules and k_{33}/k_{11} in single- as well as two-class mixtures. The lowest ratios k_{33}/k_{11} which lead to the steepest transmission characteristics and largest multiplexing rates in twist cells at a given temperature were found for non-polar, aromatic molecules comprising one heterocyclic ring.

By blending components belonging to different LC-classes we found that "elastic depressions" may occur leading to values of k_{33}/k_{11} of the mixture which are smaller than those of either of its components. From our experiments it seems that the length/width ratio of the rigid core may not influence k_{33}/k_{11} to the extent supposed so far.

Acknowledgement

We wish to acknowledge the assistance of B. Blöchliger, J. Schaufelberger and U. Witschi in the experimental work.

[1] H. Gruler, T. J. Scheffer, and G. Meier, Z. Naturforsch. **27a**, 966 (1972).
[2] W. H. De Jeu and W. A. P. Claassen, J. Chem. Phys. **67**, 3705 (1977).
[3] M. Schadt and F. Müller, IEEE Transactions **Ed15**, 1125 (1978).
[4] H. P. Schad, G. Baur, and G. Meier, J. Chem. Phys. 70, 2770 (1979).
[5] F. Leenhouts and A. J. Dekker, J. Chem. Phys. **74**, 1956 (1981)
[6] B. S. Scheuble, G. Baur, and G. Meier, Mol. Cryst. Liq. Cryst. **68**, 57 (1981).
[7] M. Schadt and F. Müller, Rev. Phys. Appl. **14**, 265 (1979).
[8] M. Schadt and W. Helfrich, Appl. Phys. Lett. **18**, 127 (1971).

[9] A. Boller and H. Scherrer, German Patent No. 2306738 (1972).
[10] A. Boller, H. Scherrer, M. Schadt, and P. Wild, Proc. IEEE **60**, 1002 (1972).
[11] G. W. Gray, K. J. Harrison, and J. A. Nash, Electron. Lett. **9**, 98 (1974).
[12] D. Demus, H. J. Deutscher, F. Kuschel, and H. Schubert, German Patent Nr. 2429093 (1973).
[13] R. Eidenschink, D. Erdmann, J. Krause, and L. Pohl, Angew. Chem. **89**, 103 (1977).
[14] These compounds were synthesized independently by three different research groups, namely H. Zaschke, H. M. Vorbroth, D. Demus, and H. Kresse, GDR Patent Nr. 139867 (1978). A. Boller, A. Germann, M. Schadt, and A. Villiger, Swiss Patent Application Nr. 10154/79 (1979). H. Sorkin, Mol. Cryst. Liq. Cryst. Lett. **56**, 279 (1980).
[15] A. Boller, M. Cereghetti, M. Schadt, and H. Scherrer, Mol. Cryst. Liq. Cryst. **42**, 215 (1977).
[16] A. Villiger, A. Boller, and M. Schadt, Z. Naturforsch. **34b**, 1535 (1979).
[17] P. R. Gerber and M. Schadt, Z. Naturforsch. **35a**, 1036 (1980).
[18] W. Maier and G. Meier, Z. Naturforsch. **16a**, 262 (1961).
[19] P. G. de Gennes, The Physics of Liquid Crystals, Claredon Press, Oxford 1974.
[20] D. W. Berreman, J. Opt. Soc. Amer. **63**, 1374 (1973).
[21] P. Gerber, Appl. Phys. **25**, 259 (1981).